Mechanics & Industry **21**, 615 (2020)
© AFM, EDP Sciences 2020
https://doi.org/10.1051/meca/2020087

Mechanics & Industry

Available online at:
www.mechanics-industry.org

Regular Article

A three-dimensional finite element-approach to investigate the optimum cutting parameters in machining AA2024

Hassan Ijaz[1], Mohd Danish[1,*], Muhammad Asad[2], and Saeed Rubaiee[1]

[1] Department of Mechanical and Materials Engineering, University of Jeddah, Jeddah 21589, Saudi Arabia
[2] Mechanical Engineering Department, Prince Mohammad Bin Fahd University, AlKhobar 31952, Saudi Arabia

Received: 27 June 2020 / Accepted: 2 November 2020

Abstract. This research work presents a numerical study of the orthogonal cutting process employing a finite element approach to optimize dry machining of aluminium alloy 2024. The main objective of the research work is to perform three-dimensional finite element simulations for a better understanding of temperature distribution and residual stresses development in the workpiece and tool regions along depth of cut direction. While, two-dimensional models don't predict true picture of aforesaid parameters along cutting depth due to material's out of plane flow and deformation. In the present study, effects of tool rake angles (7°, 14°, 21°) and cutting speeds (200, 400, 800 m/min) upon variations in chip geometry at various sections along workpiece width (depth of cut) have been discussed at large. Furthermore, cutting forces and tool-workpiece temperature profiles are also in depth analysed. The findings will lead the manufacturers to better decide post machining processes like heat treatment, deburring, surface treatments, etc. The results showed that a combination of a rake angle of 14° at cutting velocity of 800 m/min produces serrated chip segments with relatively moderate cutting forces in comparison to other parametric combinations. The efficacy of the presented finite element model is verified by comparing the numerically obtained results with experimental ones.

Keywords: Finite element analysis / damage evolution / machining process / material modelling / AA2024

1 Introduction

Aluminium alloy 2024 is used extensively in aerospace, aeronautic and automobile industry due to its excellent mechanical properties. While many of the AA2024 based structural components are machined before obtaining final designed shape. During machining processes, workpiece and cutting tool experience severe thermal and mechanical loads. The intensity of loads depends upon various machining parameters such as tool rake angle, cutting velocity, physical and mechanical properties of the machined parts, etc. The selection of the appropriate machining parameters may reduce the cutting energy requirements and improve the machined surface quality and integrity. Additionally, these optimally selected machining parameters are beneficial for the enhanced tool wear characteristics and reduced efforts of post-machining processes like deburring [1,2].

Machining experiments are normally conducted to find the optimum machining parameters and figure out tool friction and wear characteristics, etc. [3,4]. Normally machining costs are justified for mass production, however, for limited experimental campaigns the costs are quite high and time consuming. That does include multiple direct and indirect pre, post and in-process machining and energy costs. Additionally, CO_2 emission is an allied drawback of the experimental works [5–7].

Therefore, it is always desirable to find the alternate analyses solutions, like use of well-established finite element analysis approach to obtain desirable machining parameters. While, later approach for predicting machining design parameters of interest has been proved cost and time effective. Numerous authors have effectively used finite element simulations to analyze and optimize machining processes [8–10].

Most of simulation work on machining processes is based on two dimensional finite element analysis at macro-to-micro scales [11–19]. While, in some studies three dimensional finite element analysis has been performed to have broader insight into machined surface topology and tool wear profile and patterns [20–22].

Selection of optimum cutting parameters depends on the choice of workpiece and cutting tool materials and geometry, cutting conditions (dry, flooded, minimum quantity lubrication, cryogenic, laser assisted, etc.) and

* e-mail: mdanish@uj.edu.sa

machine dynamics. Therefore, it is a multifaceted task to optimize machining. Often, an optimally chosen set of cutting parameters shows promising results for enhanced tool life, but compromised machined surface or reduction in productivity and vice versa. For example, in high speed machining performed at high cutting velocities results in reduced resultant forces experienced by the tool and increased productivity but may tend to produce the serrated and segmented chips and accelerated tool wear. Whereas, serrated and segmented chip morphologies adversely affect workpiece surface finish and may also affect the tool wear [19]. On the other hand, low cutting velocities produce better machined surfaces and longer tool life but long chips (that can hinder the continuous machining process and may result in longer overall production times) and relatively large cutting forces are witnessed [18]. Likewise, variation in tool rake angles has its own pros and cons.

In this context, orthogonal cutting process is simulated employing a three-dimensional finite element model for the machining of aluminium alloy 2024 using commercial software Abaqus®/Explicit. Cutting simulations are performed for three cutting velocities and rake angles variations, while feed is kept constant for all simulations. This study will assist to understand the influence of different cutting velocities and tool rake angles upon the morphology of chip formation and cutting forces for machining of this material. One of the main objectives of the current study is to study the effect of machining parameters upon the residual stress distribution and resultant temperature generation in the workpiece body, tool and chip in the width direction (along depth of cut) of the component that otherwise is not possible to capture by two-dimensional simulations. Residual stresses generated in the workpiece body due to thermal and mechanical loadings can result in premature failure of machined components. Suitable heat treatments are normally performed for critical components to remove unwanted residual stresses so it can be safely assembled with limited chances of failure. The present study equally aims to predict the generated residual stresses along cutting depth under multiple cutting conditions such that suitable post machining heat treatment processes can be selected.

It is worth to highlight that precise definition of finite element based machining models is a challenging task, including tool and workpiece geometry modelling, elements and mesh selection, friction modelling, etc. Apart from these an important part of models is to simulate the material behaviour, especially failure of material that occurs at the interface of tool and component during the machining process [15]. The failure of material during the cutting process is represented by damage mechanics and fracture mechanics approaches. Facture mechanics approach deals with the propagation of failure of already existed discontinuities [23–26], whereas, damage mechanics approach can successfully simulate the initiation and propagation of failure in the material [27,28]. In the present work, Johnson-Cook plasticity model is coupled with damage and fracture energy to realize chip deformation and separation. This coupled damage-energy based model allows capturing the initiation of the fracture at the chip and workpiece interface; considering fracture mode I loading condition. Besides, model also permits large plastic deformation and fracture in the chip; considering mode II loading that may result in serrated and segmented chip morphology. Resultant cutting forces and chip morphology for orthogonal metal cutting of aluminium alloy 2024 as acquired from the FE-based analyses are compared with experimental results for 14° tool rake angle. While, the model is onwards exploited to present the results at 7° and 21° tool rake angles with multiple combinations of cutting speed and feed values. This is to highlight that for machining of aluminium alloys; which are categorized as easy to machine materials, generally high positive rake angles are used in industry. However, simulation results for 7° are also presented in the current work to merely discuss the relative effect of tool angle variation on the results of industrial interest. The article is organized as followed:

Section 2 contains the description of workpiece and tool geometries along with mesh and necessary boundary conditions. Onwards, mathematical details of Johnson-Cook material model and experimental procedure are presented in the section. Results obtained from finite element analysis are discussed in detail in Section 3. Finally, some concluding remarks are presented in Section 4.

2 Numerical and experimental approaches

2.1 Geometrical model, mesh, constraints and interactions

This section briefly describes the geometry and constraints of the three-dimensional model conceived to realize orthogonal metal cutting simulation in Abaqus® software (Abaqus, 6.16, Dassault Systemes, Johnston, RI, USA, 2016). Figure 1, shows the cutting tool and workpiece geometries perceived in the current work. The workpiece is fixed at the bottom. The length (L), depth of cut (width) (a_P), and height (h) of the workpiece geometry are 6, 4 and 1.4 mm respectively. A fixed value uncut chip thickness (0.4 mm) is used for all the simulations, as used in the experimental work (detailed in next section). The tool motion is blocked in Y-axis and Z-axis directions. Velocity (V_C) is imposed on the tool in X-axis direction.

To model chip separation various geometry-based "node separation" and "element deletion" techniques and fracture based techniques have been adopted in literature [9,17]. While, Subbiah and Melkote [15] using quick-stop test have shown that the chip separation occurs by fracture. In the current work, this fracture-based chip separation technique has been employed. For this purpose, the workpiece is modelled into three parts: chip, damage zone and workpiece support. Whereas, the thickness of the damage zone is taken equal to the tool tip radius ($Rn = 20\,\mu m$) [15]. The elements of this zone will be removed from the mesh once the damage evolution parameter D approaches to one.

Eight nodes coupled temperature-displacement hexahedral continuum elements (C3D8RT) are used for finite

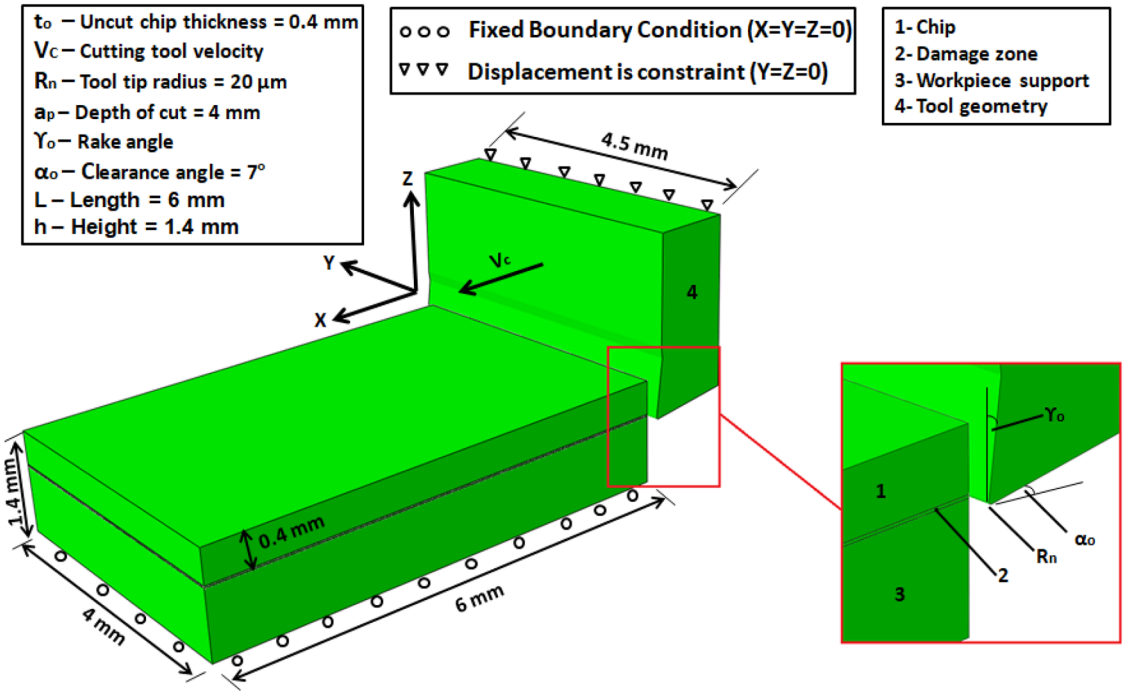

Fig. 1. Tool and workpiece geometries.

Table 1. Material properties of Tungsten Carbide Tool and AA2024 workpiece [18].

Physical parameter	Tool (Tungsten Carbide insert)	Workpiece (AA2024)
T_{melt} (°C)	–	520
T_{room} (°C)	25	25
K_{IC} (MPa$\sqrt{\text{m}}$)	–	26
K_{IIC} (MPa$\sqrt{\text{m}}$)	–	37
Expansion, α (mm^{-1}°C^{-1})	–	$\alpha + 8.9 \times 10^{-3}\ T + 2.2$
Density, ρ (kg/m^3) at 25 °C	11 900	2700
Specific heat, Cp (T) (Jkg^{-1}°C^{-1})	400	$Cp = 0.557\ T + 877.6$
Poisson ratio, ν	0.22	0.33
Thermal conductivity λ (T) (Wm^{-1}C^{-1})	50	$25 \leq T \leq 300$: $\lambda = 0.247T + 114.4$ $300 \leq T \leq T_{\text{melt}}$: $\lambda = -0.125T + 226.0$

element analysis. While, a mesh density of the order of 20 µm is chosen in different parts of tool and workpiece. The physical material properties of Tungsten Carbide Tool and AA2024 workpiece are given in Table 1. A Coulomb friction contact is defined between tool and workpiece to define frictional interaction [29–31].

To model the heat generation due to friction and inelastic work equations (1) and (2) are used. Whereas, steady state energy condition takes the form as per equation (3).

$$\dot{q}_f = \rho C_p \frac{\Delta T_f}{\Delta t} = \eta_f J \tau_f \dot{\gamma} \tag{1}$$

$$\dot{q}_p = \eta_p \overline{\sigma} \cdot \dot{\bar{\varepsilon}} \tag{2}$$

$$\lambda\left(\frac{\partial^2 T}{\partial x^2} + \frac{\partial^2 T}{\partial y^2} + \frac{\partial^2 T}{\partial z^2}\right) - \rho C_p\left(u_x \frac{\partial T}{\partial x} + u_y \frac{\partial T}{\partial y} + u_z \frac{\partial T}{\partial z}\right) \times \dot{q}_f + \dot{q}_p = 0 \tag{3}$$

2.2 Constitutive material model

Plasticity coupled thermo-mechanical behaviour of aluminium alloy can be successfully simulated by Johnson-Cook material model. The model is frequently used in literature for high speed deformation processes

Table 2. Johnson-Cook material parameters for aluminium alloy [34].

D1	*D2*	*D3*	*D4*	*D5*	m	*C*	*n*	σ_y (MPa)	*B* (Mpa)
0.13	0.13	−1.5	0.011	0	1	0.0083	0.42	352	440

like machining. If $\overline{\sigma}$ is defined as equivalent plastic flow stress, then [32]:

$$\overline{\sigma} = \underbrace{\left(\sigma_y + B\overline{\varepsilon}^n\right)}_{\text{Plastic term}} \underbrace{\left[1 + C\ln\left(\frac{\dot{\overline{\varepsilon}}}{\dot{\overline{\varepsilon}}_0}\right)\right]}_{\text{Viscosity term}} \underbrace{\left[1 - \left(\frac{T - T_{\text{room}}}{T_{\text{melt}} - T_{\text{room}}}\right)^m\right]}_{\text{Softening term}} \tag{4}$$

whereas, σ_y represents the material yield strength. While B, n, C and m are material parameters obtained from experiments for a particular material. Melting point and room temperatures are denoted by T_{melt} and T_{room} respectively. $\overline{\varepsilon}$ and $\dot{\overline{\varepsilon}}$ represent the equivalent plastic strain and the plastic strain rate respectively. $\dot{\overline{\varepsilon}}_0$ known as reference strain rate.

Johnson-Cook model defines the $\overline{\varepsilon}_{0i}$ as the equivalent plastic strain at the onset of damage as [33]:

$$\overline{\varepsilon}_{0i} = \left[D_1 + D_2\exp\left(D_3\frac{P}{\overline{\sigma}}\right)\right]\left[1 + D_4\ln\left(\frac{\dot{\overline{\varepsilon}}}{\dot{\overline{\varepsilon}}_0}\right)\right] \times\left[1 + D_5\left(\frac{T - T_{\text{room}}}{T_{\text{melt}} - T_{\text{room}}}\right)\right] \tag{5}$$

While, $D_1 - D_5$ are material damage parameters [31] and P is defined as the pressure stress. Various material parameters for aluminium alloy 2024 used in Johnson-Cook model are given in Table 2 [34]. If ω is defined as a scalar parameter then damage is initiated in the material when its value exceeds 1 [35].

$$\frac{\omega = \sum \Delta\overline{\varepsilon}}{\overline{\varepsilon}_{0i}} \tag{6}$$

The fracture energy G_f may be written as followed [36]:

$$G_f = \int_0^{\overline{u}_f} \overline{\sigma}_y d\overline{u} \tag{7}$$

In the above equation, equivalent plastic displacement $\overline{u}_f$ is defined as [37]:

$$\overline{u}_f = \frac{2G_f}{\sigma_f} \tag{8}$$

Mode I and Mode II fracture energy can be calculated by experimentally measured fracture toughness (K_{IC} and K_{IIC}) as [38]:

$$\left(G_f\right)_{I,II} = \left(\frac{1 - \upsilon^2}{E}\right)\left(K_C^2\right)_{I,II} \tag{9}$$

where υ and E represent the material's Poisson's ratio and modulus of elasticity respectively. Linear and exponential damage evolution laws are used once the damage is initiated in the material. The linear (attributed to damage section) and exponential (assigned to chip region) evolution of scalar damage variable D may be defined as [18]:

$$D = \frac{\overline{u}}{\overline{u}_f} \tag{10}$$

$$D = 1 - \exp\left(-\int_0^{\overline{u}} \frac{\overline{\sigma}}{G_f} d\overline{u}\right) \tag{11}$$

The linear and exponential evolutions of resultant stress, $\sigma = (1 - D)\overline{\sigma}$, and scalar damage variable, D, are shown in Figure 2.

As "D" approaches to "one" in workpiece elements, especially in "damage" area that experience sever thermo-mechanical loadings; elements' stiffness fully degrades and the element is removed from the mesh. Accordingly, chip separation from workpiece is perceived. While, in chip, thermo-mechanical loadings are not very high as in "damage" area of workpiece, therefore, "D" value never accumulates to numeric value of "one" in chip. The material in chip region remains intact and is not removed from mesh. However, deformation in deformed chip elements causes changes in chip morphology, like evolution from continuous to highly segmented chip.

2.3 Experimentation

To realize orthogonal cutting on lathe machine (Universal Lathe Gallic 20, Mondiale Gallic, Netherlands), the shape of the test piece has been defined to satisfy the assumptions of orthogonal cutting as shown in Figure 3. Initially a bore has been made in an aluminum bar (Material: AA2024) to give the cutting width (a_P). To ensure stiffness of workpiece during machining and to avoid any vibration of the work-part, the depth of the groove was reduced to a minimum. To avoid the curvature of the part in the simulation model and to obtain the highest possible cutting speed a fairly large diameter Ø150 mm of the test piece has been chosen.

Cutting insert (CCGX 12 04 08-AL H10, Sandvik, Sweden) mounted on Sandvik's insert holder (SCLCR 2020K 12 Sandvik, Sweden) is used to perform the machining operation. This uncoated carbide insert has a strongly positive cutting rake angle (14°) and is recommended for machining of aluminium alloys. To reproduce orthogonal cutting conditions, the insert cutting edge was orthogonal with feed and cutting speed.

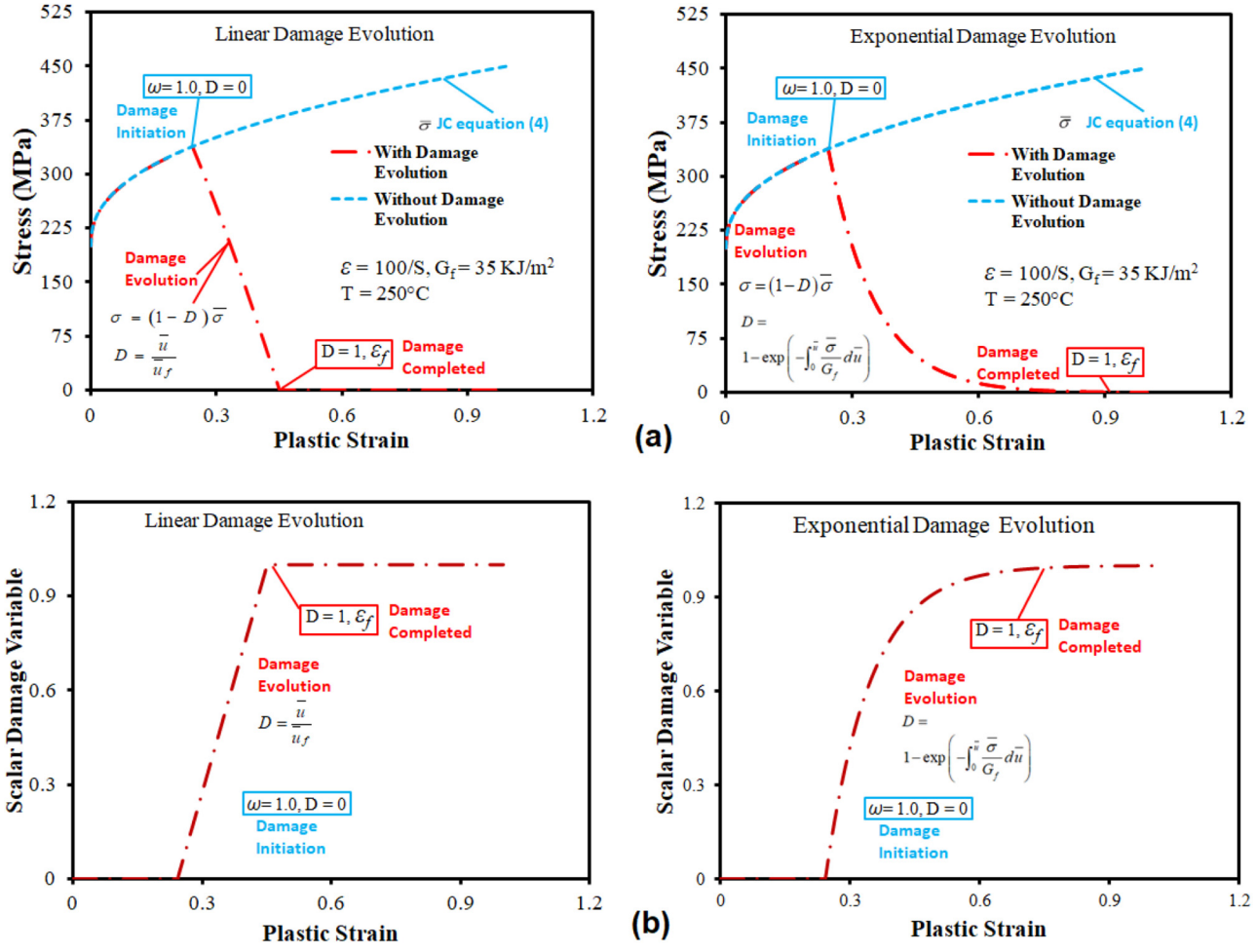

Fig. 2. Linear and exponential damage evolution. (a) Stress-strain behaviour (b) Scalar damage variable D.

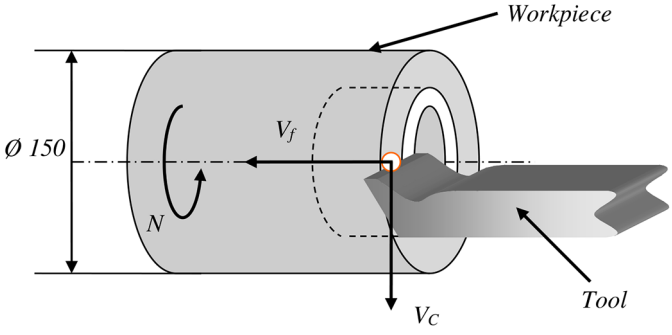

Fig. 3. Workpiece preparation for orthogonal machining.

Kistler "9257B" dynamometer, Kistler "5015A" charge amplifiers and National Instrument "NI 4472" data acquisition devices have been used to register and analyse the cutting forces. Orthogonal cutting operations performed for cutting velocities: 200, 400 and 800 m/min for fixed uncut chip thickness (t_o): 0.4 mm (feed) and constant depth of cut (a_P): 4 mm. Onwards, chips were acquired, treated (entrenched in allylic resin, polished and etched with 4% nitric acid solution) and photographed using scanning electron microscope to visualize the final geometry of chips. It can be seen in Figure 4 that more discreet height of the serrations is observed on the chip as the cutting speed is increased.

3 Results and discussions

The results obtained from finite element analysis are presented and discussed here. Figure 5 shows the evolution of cutting force for various rake angles for cutting speed of 800 m/min. In depth analysis of Figure 5 depicts that resultant cutting force increases as the tool rake angle decreases, while similar trend has also been reported previously by Asad [18]. This is to recall that experimental work was performed considering rake angle of 14° only at all three cutting speeds (200, 400 and 800 m/min), keeping feed value constant ($f = 0.4$ mm/rev). Accordingly, experimental data related to cutting forces and chip morphology has been acquired and same is compared with analysis results at various levels to validate the proposed FE based cutting model. The cutting forces (at 14° rake angle) are in close agreement with the average experimental results. The results of cutting forces for 7° and 21° are also in accordance

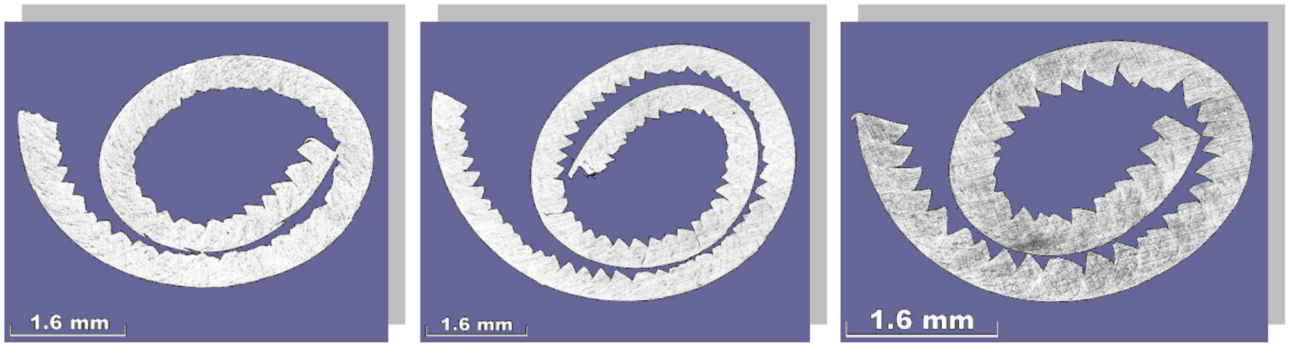

Fig. 4. Analysis by electron microscope ($f = 0.4$ mm/rev) (from left to right: $V_C = 200$, 400, 800 m/min).

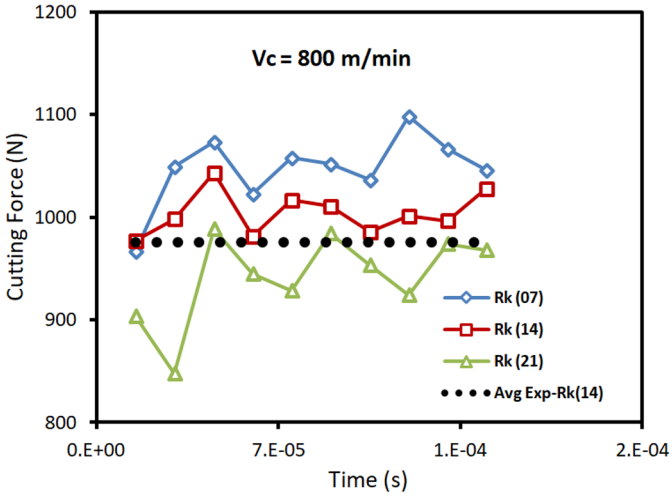

Fig. 5. Evolution of cutting force with time for various tool rake angles for fixed 800 m/min cutting speed.

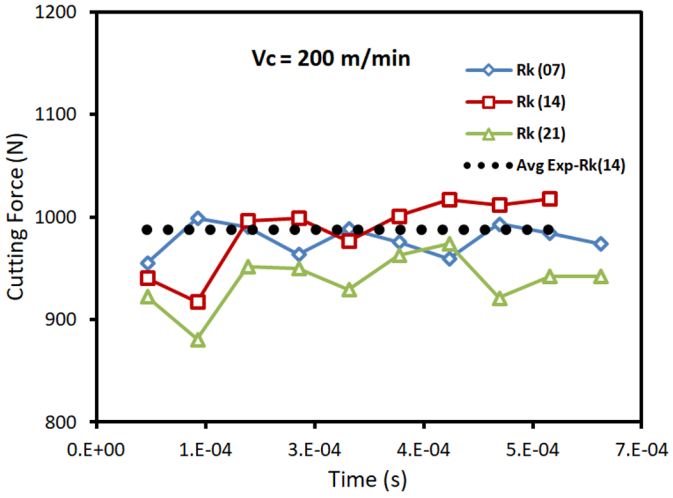

Fig. 6. Evolution of cutting force with time for various tool rake angles for fixed 200 m/min cutting speed.

with general machining trend. However, fluctuations in the cutting force (up to ±50 N) can be clearly marked. Dynamic contact condition, damage initiation and propagation, chip segmentation are the possible reasons for this fluctuation in the cutting forces. These fluctuations in the cutting forces are not only detrimental and may result in accelerated tool wear leading to premature tool failure under potential fatigue load, but may also result in compromised machined surface roughness [18]. Similar trends can also be figured out in Figure 6, showing results at comparatively lower speed of 200 m/min, though, force fluctuations are now decreased.

This is to highlight that with chosen range of cutting speeds, no considerable change in cutting forces has been found, as per Figure 7. This seems commensurate with general high speed machining concepts, that in high-speed machining (where cutting speed values are normally taken at more than 1200 m/min for aluminium alloys) lower cutting forces results due to softening of materials. However, a slight increasing trend in cutting forces can be marked as cutting forces increases. This may be attributed to strain rate dependent properties of this material.

Chip morphologies are also plotted for various combinations of cutting parameters and provide interesting

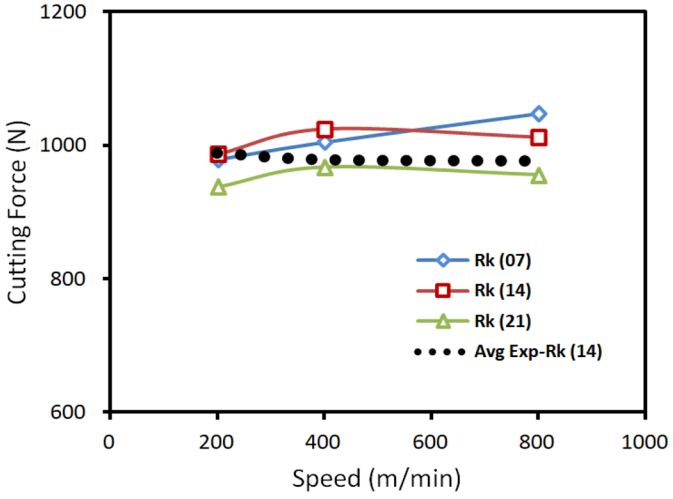

Fig. 7. Variation of cutting force with cutting speed for various tool rake angles.

results. Generally, higher cutting speed with lower rake angle promotes generation of segmented chip morphologies, as shown in Figure 8. While higher rake angles with lower cutting speeds result in continuous chip morphologies (Fig. 9).

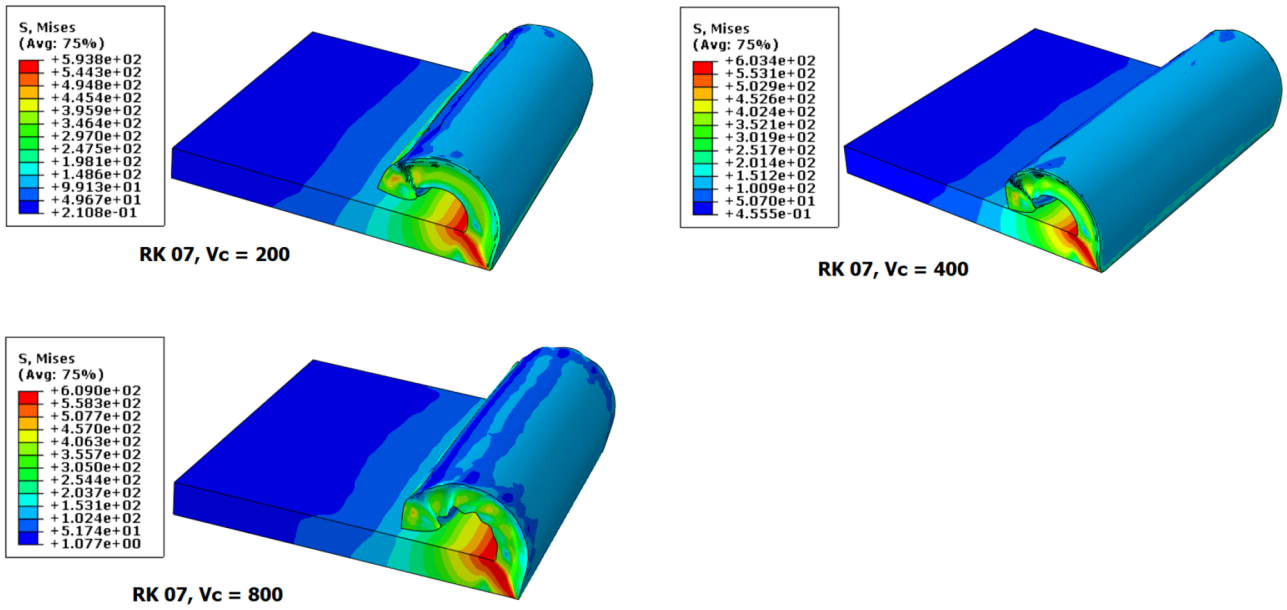

Fig. 8. Chip morphologies for various cutting speeds with a fixed rake angle of 7°.

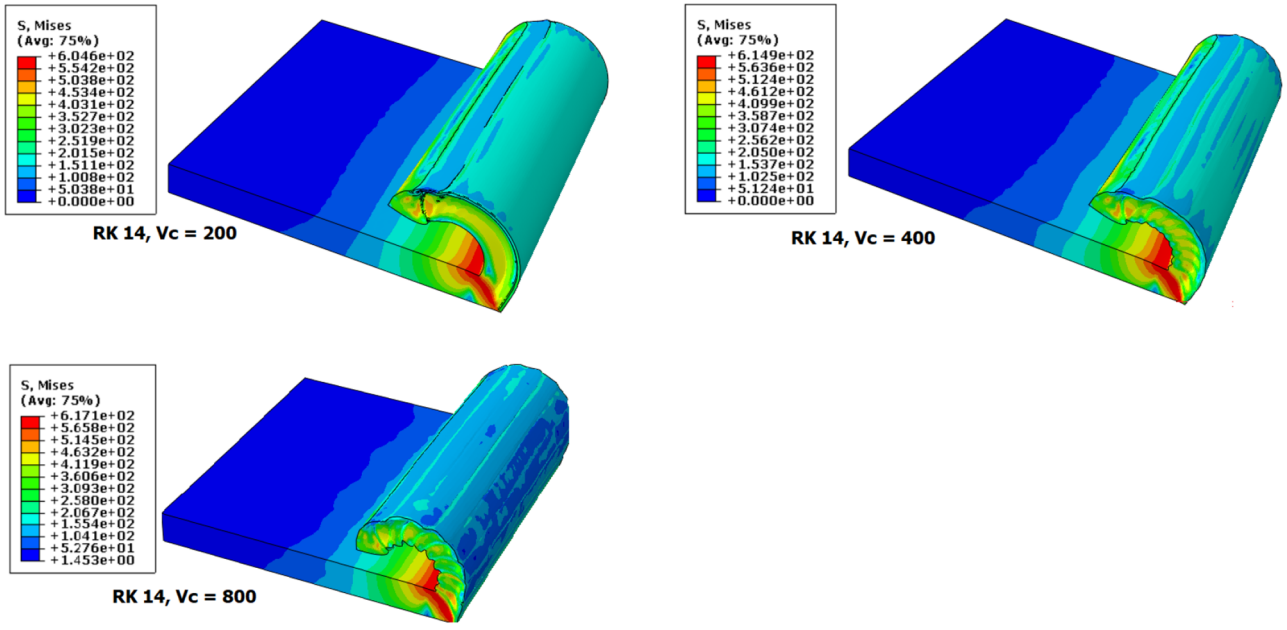

Fig. 9. Chip morphologies for various cutting speeds with a fixed rake angle of 14°.

It is therefore recommended to use positive rake angles with lower cutting speeds, Figures 8 and 9, to generate continuous and smoother surfaces and longer tool lives, though it can decrease the production rate. In fact, combination of lower rake angles and high cutting speeds increase tool-chip interface temperatures. This in turn promotes thermal softening and ease in flow of material in cutting direction. Under severe thermal loading conditions, damage in the material initiates and evolves (Equs. (6), (10) and (11)). This generates the highly stressed chip segments. When damage parameter approaches 1.0, chip fragmentation occurs [19]. Contrary, high positive rake angles and low cutting speed combinations do not produce severe thermo-mechanical loading in chip and workpiece materials. Eventually, smoother chip morphology (more continuous and less segmented) is resulted, as depicted in Figure 9. Several studies [19,20] show that continuous chip morphology dictates smoother and less undulated machined surface finish profiles. Continuous chip also results in reduced longitudinal residual stresses on machined surface in contrast to undulated surface produced because of highly segmented chip morphology [39].

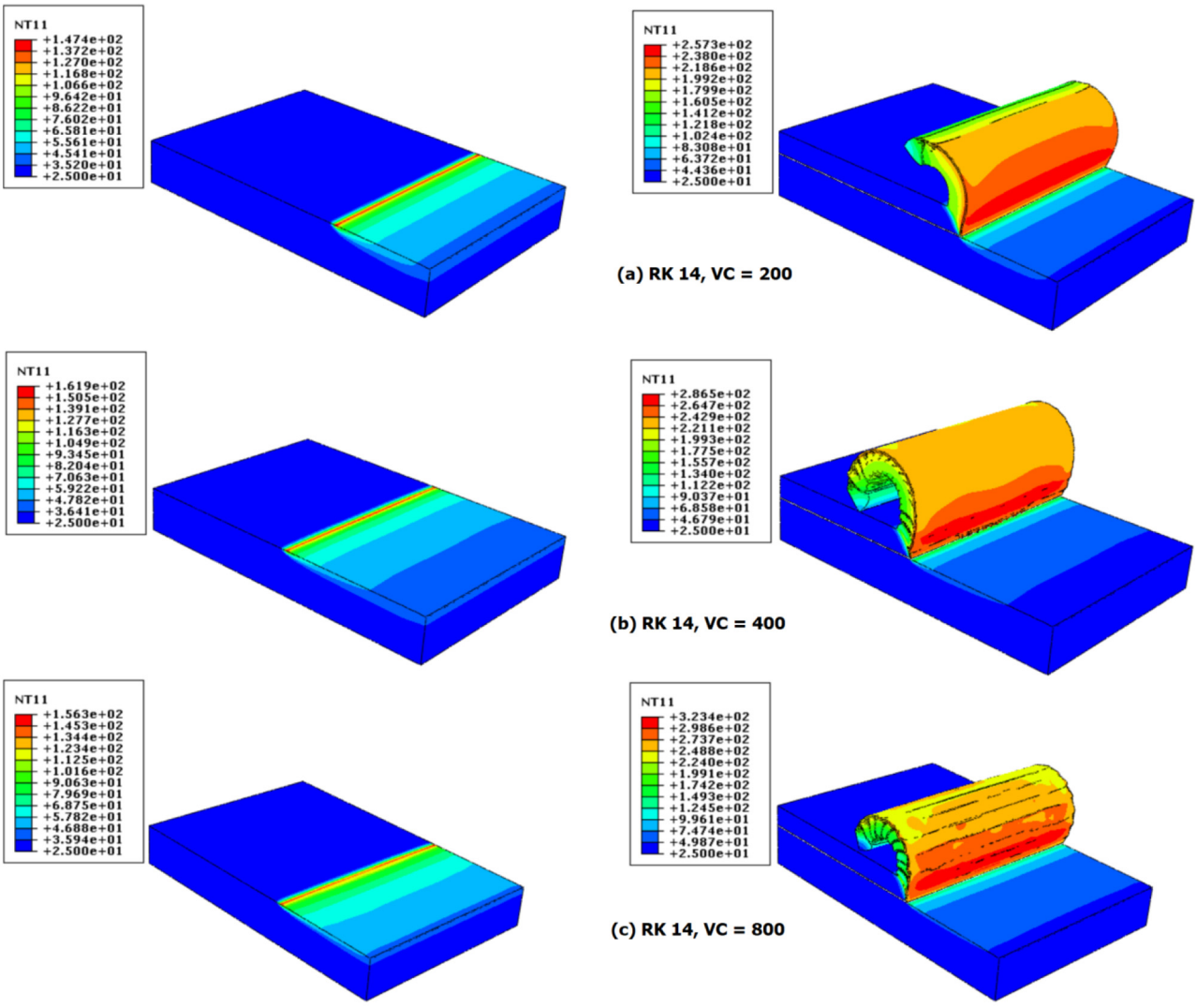

Fig. 10. Temperature profiles of chip and workpiece with Rake angle of 14° at different.

It is worth mentioning that segmented chip not only effect the machined surface integrity (surface profile and residual stress) but may also affect the tool life. Machined surface nodes oscillate with higher amplitudes during elastic recovery of the machined material. These nodes strike the tool flake face with higher elastic potential energy and increase the risk of early tool failure because of speedy tool flank wear. Tool's crater wear might also pronounce because of non-uniform chip morphology [19].

Figure 10, shows the simulated temperature profiles in chip and machined workpiece sections for three different cutting speeds with a rake angle of 14°. Temperature profiles indicate that maximum temperature rises in the chip as the cutting speed increases. On the other hand, non remarkable temperature rise was noticed in the workpiece geometry with an increase in cutting speed [40]. This lies in good agreement with general machining theory that around 80% of heat is carried by chip, while remaining is contained by tool and machined work part. The higher temperatures in chip may be attributed to large plastic deformation when compared with workpiece.

Figure 11, depicts the variations in temperature for chip and workpiece geometries with multiple rake angle for different cutting speeds. It can be noticed from the graph that there is a small variation in temperature in the workpiece geometry as the rake angle changes for various cutting speeds. Nevertheless, it is clearly visualized that the temperature rises considerably in the chip as the cutting speed increases for a particular value of tool rake angle. Later fact can be attributed to higher frictional resistance at higher cutting velocities on the tool rake face. Marginal variations in temperature can also be observed by changing the tool rake angle at particular cutting speed. Similar trends have also been reported in the work of Waqas et al. [40].

Figure 12, shows two different x-sections of the chip along the width direction (400 m/min, 14° Rake angle). One can observe that the more serrations on the outer x-section, that is, on the workpiece edge. These higher

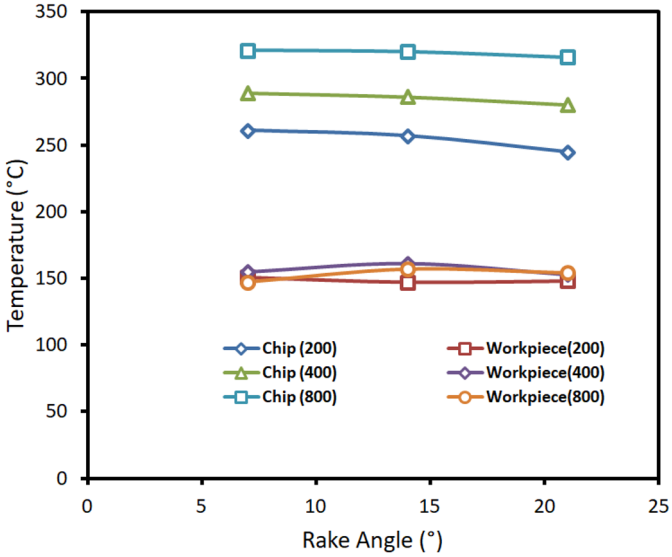

Fig. 11. Predicted temperature in chip and workpiece with tool rake angles for different cutting speeds.

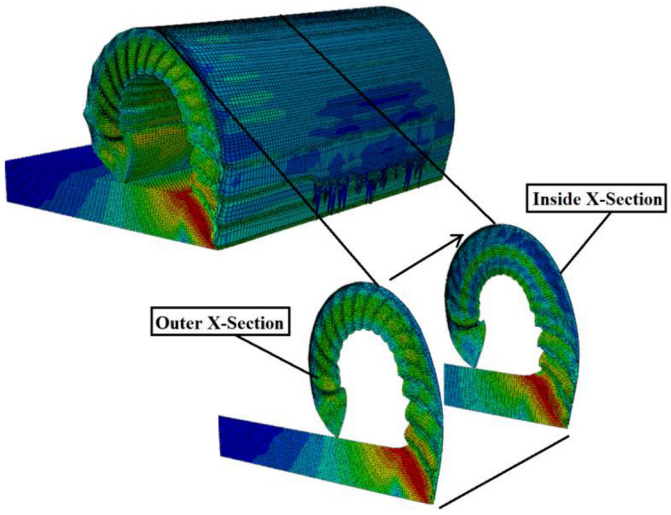

Fig. 12. Simulated chip geometry at various x-sections along the width direction.

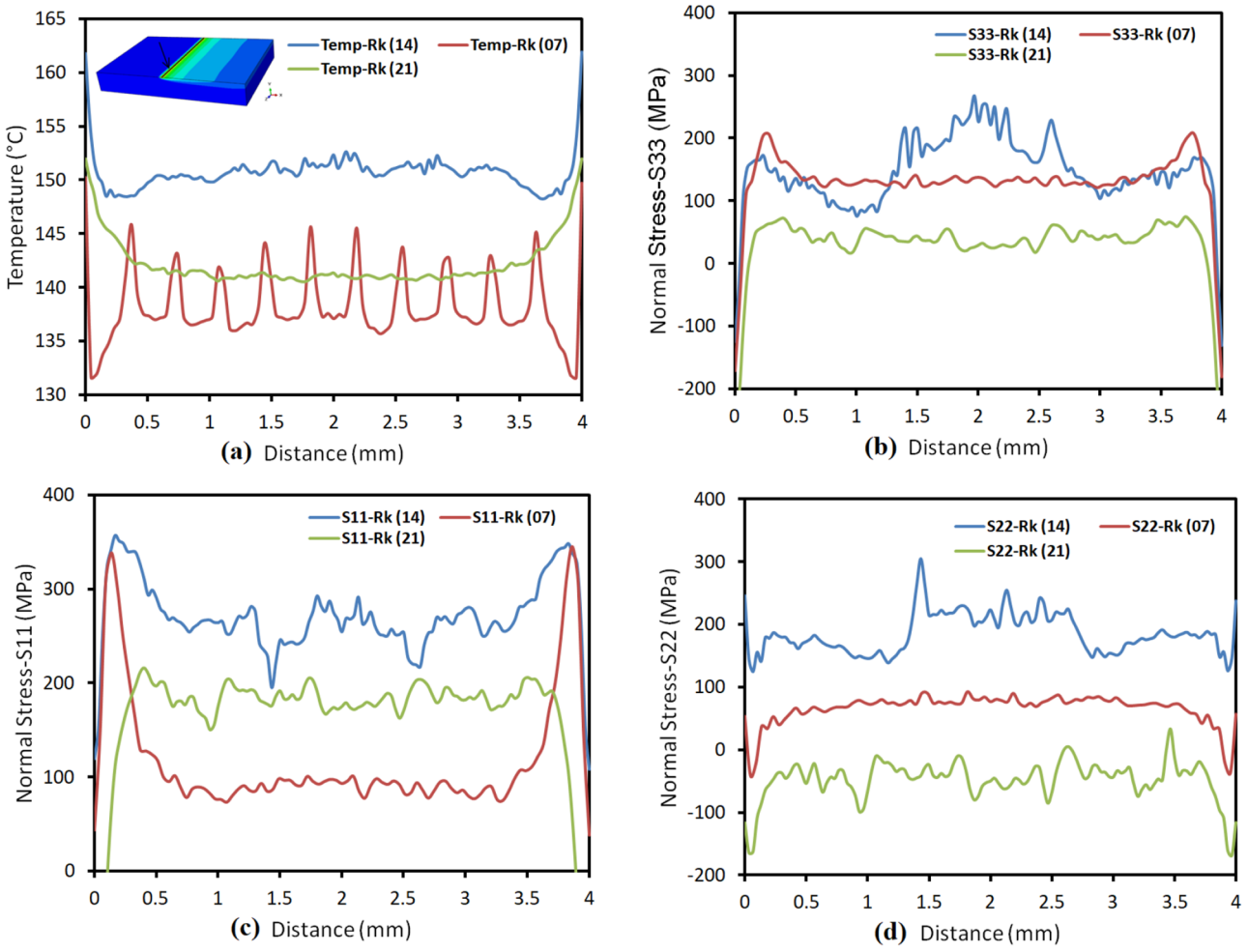

Fig. 13. Predicted variations of Temperature and Normal stresses along the width of the Workpiece geometry for different values of rake angles.

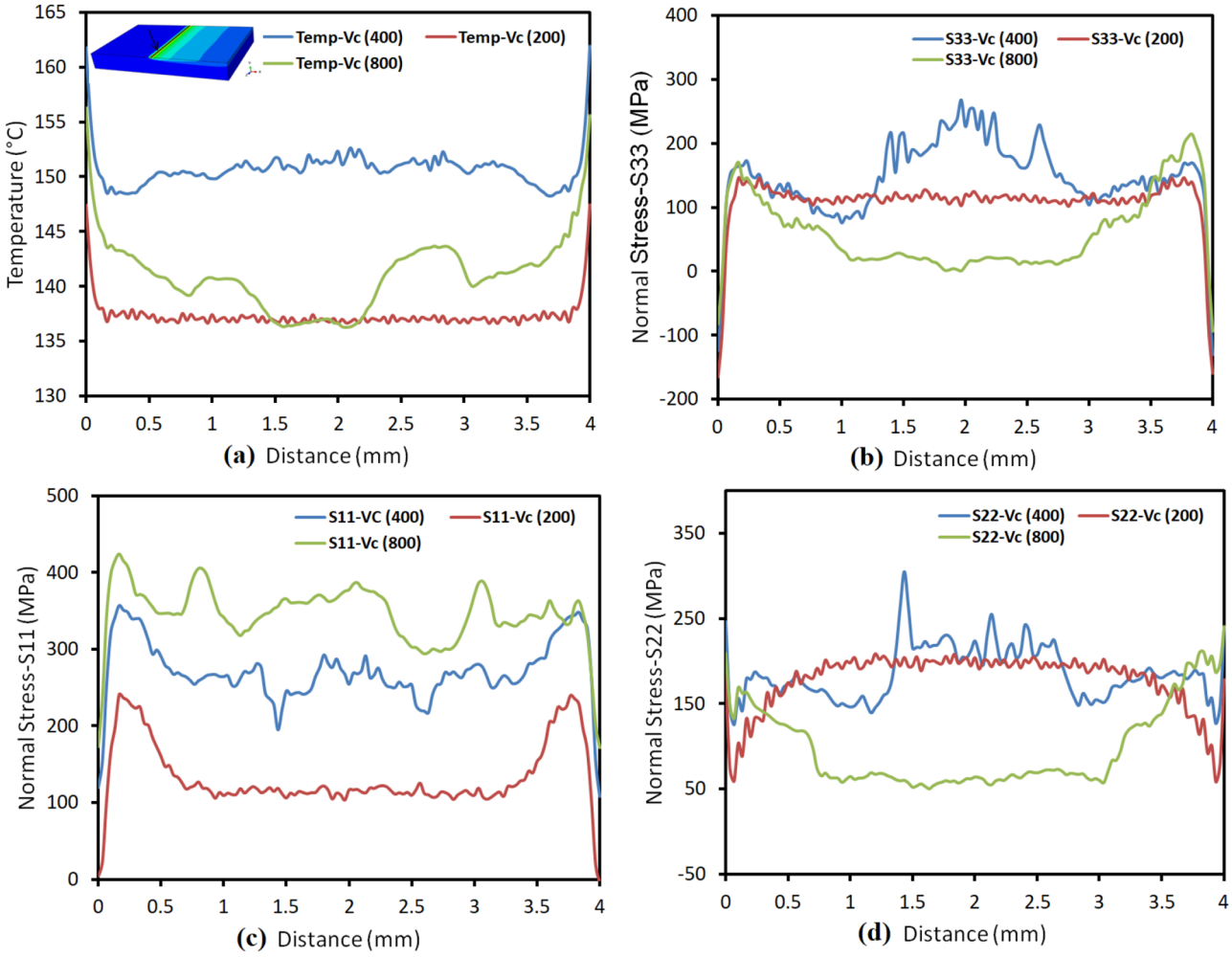

Fig. 14. Predicted variations of Temperatures and Normal stresses along the width of the Workpiece geometry for different values of cutting speeds.

numbers of serrations may be attributed to the outward material flow during the machining process. It will not be possible to get these details with two-dimensional finite element simulations along the depth of cut (width).

Figure 13, presents the variations of the temperatures and normal stresses along the width of the workpiece geometry with different values of rake angles while keeping cutting speed constant at 400 m/min. Higher temperature values at the extreme outer ends of the workpiece geometry (Fig. 13a) can be spotted. These high temperatures may result in loss of stiffness in these regions and that may cause edge damage and side burr formation. Similarly, plots of normal stresses are shown along the width direction and variation of the stress values can be marked. Likewise, same behaviours are observed when temperature and normal stress profiles have been plotted for different cutting speeds, as per Figure 14. These clearly indicate that the temperatures and stresses variations along the width.

Figure 15, displays the effect of material flow in width (depth of cut) direction considering varying values of rake angles and cutting speeds. Higher deformation values predicted at the outer edges of the workpiece geometry. These deformation values may help to evaluate burr formation under different machining conditions. High positive tool rake angles with low cutting speeds tend to reduce the burr formations in the machined parts [39].

During machining of structural parts, cutting tools experience severe thermal and mechanical loads. Higher load values may influence and thus reduce the tool life by increasing the wear.

Figure 16, depicts the variation of temperatures experienced by the tool surface during the machining with different values of cutting speeds and tool rake angles. This variation of temperature on the cutting surface of the tool is almost constant along the width direction during cutting operation, while higher temperatures are resulted at higher cutting speeds. Furthermore, highest cutting temperatures at a rake angle of 14° are witnessed.

Additionally, chip morphology has been greatly affected by the choice of cutting speeds and tool rake angles (Figs. 17 and 18). Temperatures and outward deformations for different tool rake angles are sown in Figure 17. Repeatedly, it can be noticed that both of these results vary along the width direction. The variation of deformation

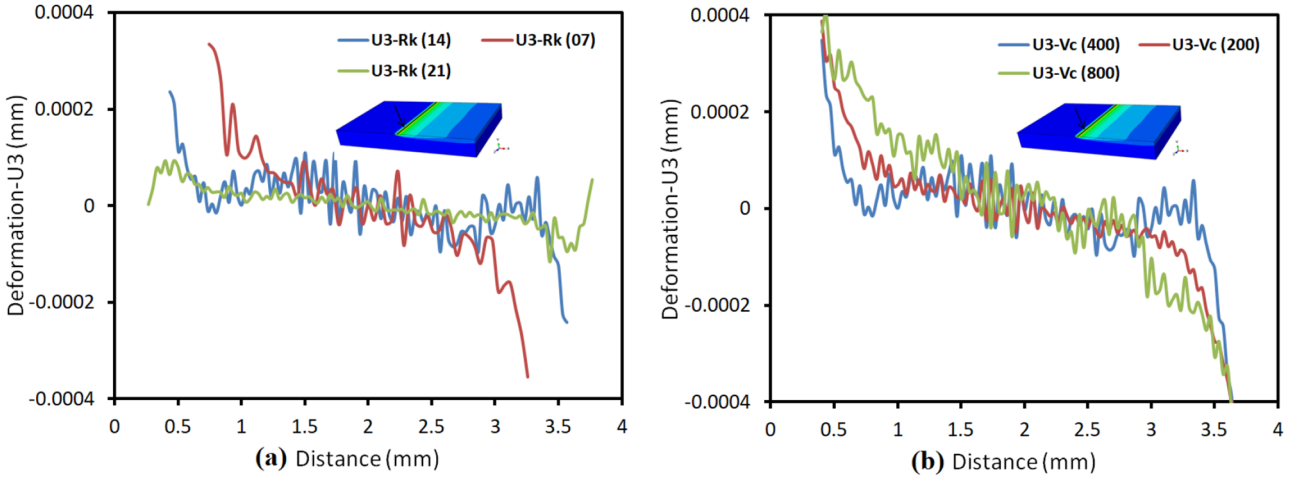

Fig. 15. Predicted values of deformations along the width of the Workpiece geometry for different values of tool rake angles and cutting speeds.

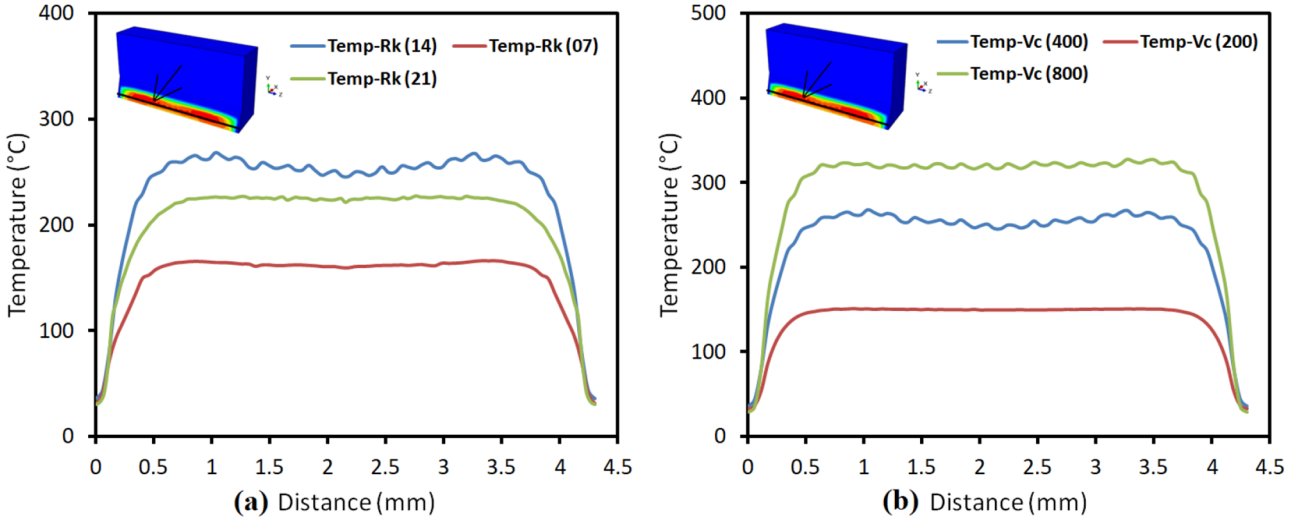

Fig. 16. Predicted values of temperatures along the width of the Tool for different values of tool rake angles and cutting speeds.

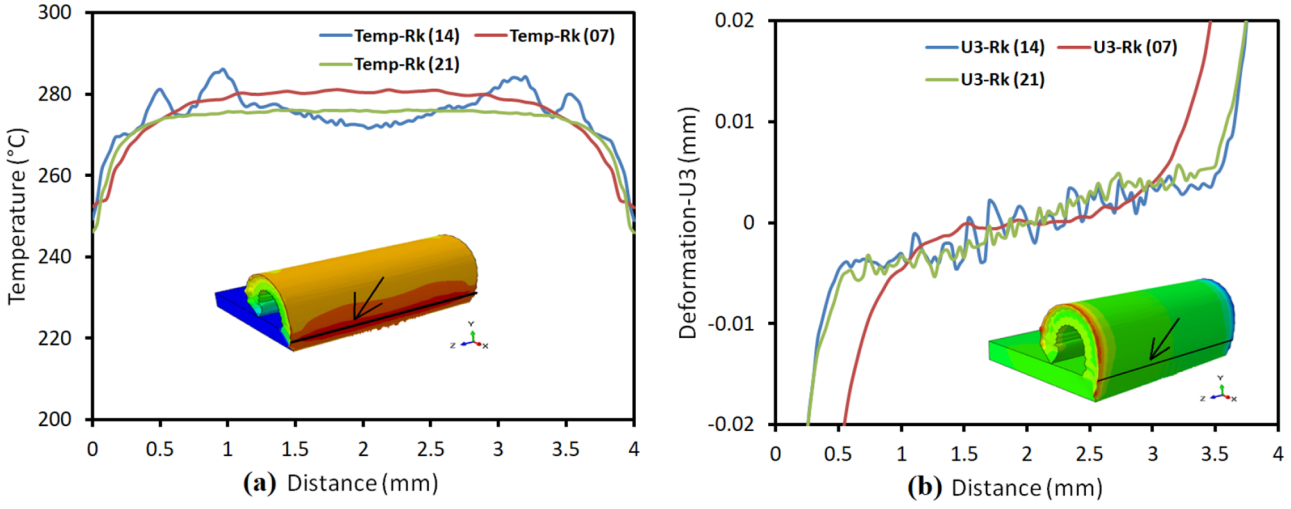

Fig. 17. Predicted values of temperatures and deformations along the width of the Chip for different values of rake angle.

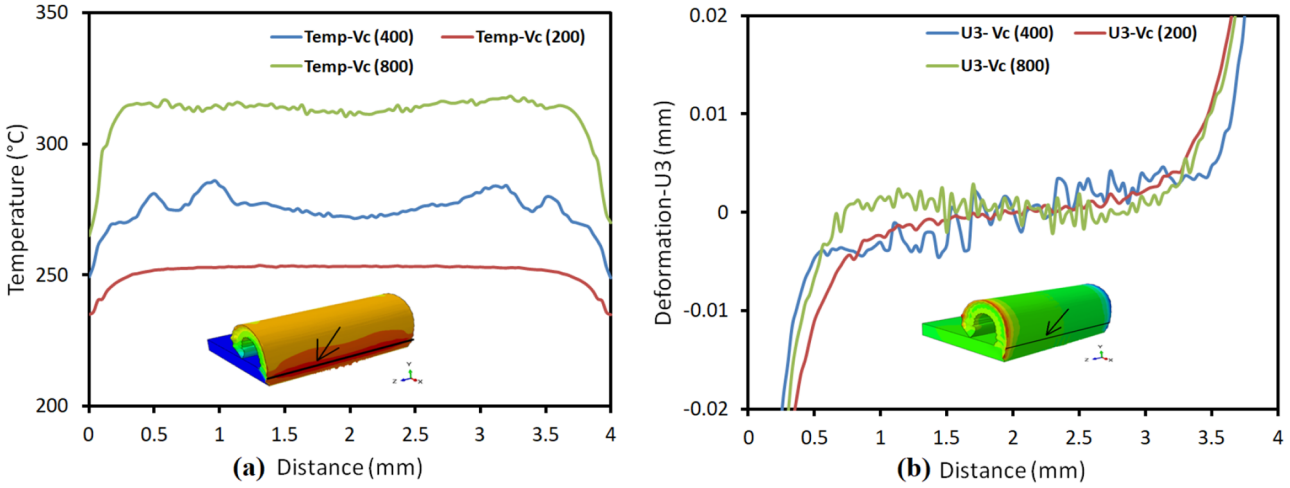

Fig. 18. Predicted values of temperatures and deformations along the width of the Chip for different cutting speeds.

presents the material outward flow during the machining process. There is a noticeable deformation at the outer edges of the chip. Similar type of trends observed for both, temperatures and deformations, when plotted by varying the cutting speeds (Fig. 18). From previous discussion on the acquired analysis results one can find that the three-dimensional finite element simulations can effectively predict the variations of loads along the width directions of the workpiece and cutting tool. On the other hand, two-dimensional finite element based simulations are unable to predict these variations in thermal and mechanical loads. Therefore, three-dimensional finite element analysis may effectively help to determine the optimum machining parameters by comparing the predicted cutting forces, temperatures, stresses and deformations, etc.

Finally, it can be summarized that a combination of a tool rake angle of 14° at cutting velocity of 800 m/min produces serrated chip segments with relatively moderate values of residual stresses and resultant cutting forces in dry machining of AA2024, though relatively higher temperatures on tool are observed at 14°. Furthermore, non-uniform machined surface profile at various sections along the depth of cut has been predicted.

4 Conclusion

In this article, three-dimensional finite element investigations are made to find out the optimum machining parameters aiming at machined surface integrity in terms of residual stresses profile for orthogonal cutting of AA2024. Simulations are performed considering different rake angles and cutting speeds. Simulation results show that higher cutting speeds with relatively lower rake angles tend to produce serrated chip segments and can result in poor surface finish. Contrary, lower cutting speeds with comparatively high positive rake angles may help to produce better surface finish with less surface undulations. This also helps to reduce the tool wear. Smooth surfaces and chip morphologies are related with lower thermo-mechanical loading in the later case. Less wear and smooth surfaces will result in achieving the targets of sustainable manufacturing. Additionally, maximum temperatures were predicted in the chip and workpiece geometries for various cutting speeds and different tool rake angles. It may be observed that variation in cutting speed affects the temperatures more than the tool rake- angles variations. Moreover, three-dimensional finite element analyses have helped to capture the thermal and mechanical load variations along the width directions. It has been found that at workpiece edges out of plane material flow may result in edge damage and side burr formation. Later, results are difficult to predict using two-dimensional finite element analysis approach. For example, 10–15% higher residual stresses are reported at edges than those predicted at the middle section of workpiece. Moreover, serrated chip segments with relatively moderate cutting forces obtained from finite element simulations for a rake angle of 14° at cutting velocity of 800 m/min. It is expected that results may help industrial engineers to have a better picture of non-uniform results along workpiece width, while selecting for appropriate post machining techniques and methods including deburring, stress relaxation, finishing, surface coating, etc.

Nomenclature

a_P	Depth of cut (mm)
B	Hardening modulus (MPa)
C	Strain rate dependency coefficient
Cp	Specific heat ($J.kg^{-1}{}^{\circ}C^{-1}$)
D	Damage evolution parameter
$D_1 \sim D_5$	Coefficients of Johnson-Cook material shear failure initiation criterion
E	Young's Modulus (MPa)
t_o	Uncut chip thickness (feed) (mm)
G_f	Fracture energy ($kJ.m^{-2}$)
K_{IC}	Mode I fracture toughness ($MPa.m^{1/2}$)
K_{IIC}	Mode II Fracture toughness ($MPa.m^{1/2}$)
m	Thermal softening coefficient
n	Work-hardening exponent

P	Hydrostatic pressure (MPa)
T	Temperature at a given calculation instant (°C)
T_{room}	Reference ambient temperatures (°C)
T_{melt}	Melting temperatures (°C)
$\overline{u}$	Equivalent plastic displacement (mm)
$\overline{u}_f$	Equivalent plastic displacement at failure (mm)
V	Cutting speed (m.min^{-1})
α	Coefficient of thermal expansion ($\mu\text{m.mm}^{-1}\text{°C}^{-1}$)
$\overline{\varepsilon}$	Equivalent plastic strain
$\dot{\overline{\varepsilon}}$	Plastic strain rate
$\dot{\overline{\varepsilon}}_0$	Reference strain rate ($10^{-3}.\text{s}^{-1}$)
$\overline{\varepsilon}_{0i}$	Plastic strain at damage initiation
λ	Thermal conductivity ($\text{W.m}^{-1}\text{°C}^{-1}$)
ν	Poisson's ratio
ρ	Density (kg.m^{-3})
σ	Stress (MPa)
σ_y	Yield strength (MPa)
σ_0	Friction stress (MPa)
$\overline{\sigma}$	Equivalent plastic stress (MPa)
ω	Damage initiation criterion
$\dot{q}_p$	Heat generation rate due to plastic deformation (W/m^3)
$\dot{q}_f$	Heat generation rate due to friction (W/m^3)
η_p	Inelastic heat fraction
η_f	Frictional work conversion factor
J	Fraction of heat in chip
τ_f	Shear stress
$\dot{\gamma}$	Slip strain rate

Conflict of interest

The authors declare no Conflict of interest.

This research was funded by the Deanship of Scientific Research (DSR), University of Jeddah, Jeddah, with grant No. UJ-02-005-DR. Authors are also thankful to Pr. Dr Tarek Mabrouki (University of Tunis El Manar, Tunis, Tunisia) for his fruitful discussions on numerical modelling.

References

[1] S.K. Pattnaik, N.K. Bhoi, S. Padhi, S.K. Sarangi, Dry machining of aluminum for proper selection of cutting tool: tool performance and tool wear, Int. J. Adv. Manuf. Technol. **98**, 55–65 (2018)

[2] T. Régnier, G. Fromentin, B. Marcon, J. Outeiro, A. d'Acunto, A. Crolet, T. Grunder, Fundamental study of exit burr formation mechanisms during orthogonal cutting of AlSi aluminium alloy, J. Mater. Process. Technol. **257**, 112–122 (2018)

[3] S. Werda, A. Duchosal, et al., Effect of minimum quantity lubrication strategies on tribological study of simulated machining operation, Mech. Ind. **20**, 624–630 (2019)

[4] W. Frifita, S.B. Salem. et al., Optimization of machining parameters in turning of Inconel 718 Nickel-base super alloy, Mech. Ind. **21**, 203 (2020)

[5] M. Helu, B. Behmann, H. Meier, D. Dornfeld, G. Lanza, V. Schulze, Total cost analysis of process time reduction as a green machining strategy, in: Leveraging technology for a sustainable world, pp. 299–304, Springer, Berlin, Heidelberg (2012)

[6] S. Anderberg, S. Kara, Energy and cost efficiency in CNC machining. The 7th CIRP Conference on Sustainable Manufacturing, Chennai, India (2009)

[7] A. Das, S.R. Das, S.K. Patel, B.B. Biswal, Experimental investigation of various machining attributes and cost estimation during machining of hardened AISI 4340 steel with untreated and cryo treated cermet inserts, Mech. Ind. **21**, 110 (2020)

[8] G. Liu, C. Huang, R. Su, T. Özel, Y. Liu, L. Xu, 3D FEM simulation of the turning process of stainless steel 17-4PH with differently texturized cutting tools, Int. J. Mech. Sci. **155**, 417–429 (2019)

[9] F. Salvatore, T. Mabrouki, H. Hamdi, The use of numerical simulations to improve a new analytical chip formation model, Mech. Ind. **13**, 405–414 (2012)

[10] J.C. Outeiro, D. Umbrello, R. M'Saoubi, I.S. Jawahir, Evaluation of present numerical models for predicting metal cutting performance and residual stresses, Mach. Sci. Technol. **19**, 183–216 (2015)

[11] H. Ijaz, M. Zain-ul-abdein, W. Saleem, M. Asad, T. Mabrouki, Numerical simulation of the effects of elastic anisotropy and grain size upon the machining ofAA2024. Mach. Sci. Technol. **22**, 522–542 (2018)

[12] C.J. Yin, Q.C. Zheng, Y.H. Hu, Finite element simulation of Titanium alloy turning process, Appl. Mech. Mater. **391**, 14–17 (2013)

[13] N. Tounsi, T. El-Wardany, Finite element analysis of chip formation and residual stresses induced by sequential cutting in side milling with microns to sub-micron uncut chip thickness and finite cutting edge radius, Adv. Manuf. **3**, 309–322 (2015)

[14] X. Lai, H. Li, C. Li, Z. Lin, J. Ni, Modelling and analysis of micro scale milling considering size effect, micro cutter edge radius and minimum chip thickness, Int. J. Mach. Tools Manuf. **48**, 1–14 (2008)

[15] S. Subbiah, S.N. Melkote, Effect of finite edge radius on ductile fracture ahead of the cutting tool edge in micro-cutting of Al2024-T3, Mater. Sci. Eng. A **474**, 283–300 (2008)

[16] Y. Zhang, J.C. Outeiro, T. Mabrouki, On the selection of Johnson-Cook constitutive model parameters for Ti-6Al-4 V using three types of numerical models of orthogonal cutting, Procedia CIRP. **31**, 112–117 (2015)

[17] A. Shrot, M. Baker, Determination of Johnson-Cook parameters from machining simulations, Comput. Mater. Sci. **52**, 298–304 (2012)

[18] M. Asad, Elaboration of concepts and methodologies to study peripheral down-cut milling process from macro-to-micro scales, PhD Dissertation, INSALyon, France, 2010

[19] T. Mabrouki, F. Girardin, M. Asad, J.-F. Rigal, Numerical and experimental study of dry cutting for an aeronautic aluminium alloy (A2024-T351), Int. J. Mach. Tools Manuf. **48**, 1187–1197 (2008)

[20] M. Asad, T. Mabrouki, H. Ijaz, M.A. Khan, W. Saleem, On the turning modeling and simulation: 2D and 3D FEM approaches, Mech. Ind. **15**, 427–434 (2014)

[21] T. Ozel, I. Llanos, J. Soriano, P.J. Arrazola, 3D finite element modelling of chip formation process for machining Inconel 718: comparison of FE software predictions, Mach. Sci. Technol. **15**, 21–46 (2011)
[22] J. Díaz-Álvarez, J.L. Cantero, H. Miguélez, X. Soldani, Numerical analysis of thermomechanical phenomena influencing tool wear in finishing turning of Inconel 718, Int. J. Mech. Sci. **82**, 161–169 (2014)
[23] P. Ståhle, A. Spagnoli, M. Terzanob, On the fracture processes of cutting, Procedia Struct. Integr. **3**, 468–476 (2017)
[24] J.G. Williams, Y. Patel, Fundamentals of cutting, Interface Focus **6**, 20150108 (2016)
[25] Y. Gao, J.H. Ko, H.P. Lee, Meso-scale tool breakage prediction based on finite element stress analysis for shoulder milling of hardened steel, J. Manuf. Process. **55**, 31–40 (2020)
[26] L.J. Ma, A.B. Yu, J. Chen, Theoretical model of cutting force in turning the lithium disilicate glass-ceramic, Int. J. Adv. Manuf. Technol. 1–12 (2017)
[27] Y. Su, S. Yu, S. Li, Y. He, Review of the damage mechanism in wind turbine gearbox bearings under rolling contact fatigue, Front. Mech. Eng. **14**, 434–441 (2019)
[28] H. Ijaz, Mathematical modelling and simulation of delamination crack growth in glass fiber reinforced plastic (GFRP) composite laminates, J. Theor. App. Mech. **57**, 17–26 (2019)
[29] A. Malakizadi, K. Hosseinkhani, E. Mariano, E. Ng, A. Del Prete, L. Nyborg, Influence of friction models on FE simulation results of orthogonal cutting process, Int. J. Adv. Manuf. Tech. **88**, 3217–3232 (2017)
[30] A.P. Markopoulos, N.E. Karkalos, N.M. Vaxevanidis, D.E. Manolakos, Friction in orthogonal cutting finite elements models with large negative rake angle, Tribol. Ind. **38** (2016)
[31] X. Zhang, S. Wu, H. Wang, C.R. Liu, Predicting the effects of cutting parameters and tool geometry on hard turning process using finite element method, J. Manuf. Sci. E-T ASME **133**, 041010 (2011)
[32] A.M. Bragov, V.V. Balandin, A.Y. Konstantinov, A.K. Lomunov, I.V. Vorobtsov, A.V. Kuznetsov, G.G. Savenkov, High-rate deformation and spall fracture of some metals, Procedia Eng. **197**, 260–269 (2017)
[33] F. Wang, Q. Tao, L. Xiao, J. Hu, L. Xu, Simulation and analysis of serrated chip formation in cutting process of hardened steel considering ploughing-effect, J. Mech. Sci. Technol. **32**, 2029–2037 (2018)
[34] X. Teng, T. Wierzbicki, Evaluation of six fracture models in high velocity perforation engineering, Fract. Mech. **73**, 1653–1678 (2006)
[35] Z.Y. Han, X.G. Huang, Y.G. Cao, J.Q. Xu, A non linear cumulative evolution model for corrosion fatigue damage, J. Zhejiang Univ. Sci. A **15**, 447–453 (2014)
[36] Y. Choi, H. Kim, Development of a cohesive zone model for fatigue crack growth, Multiscale Sci. Eng. **2**, 42–53 (2020)
[37] T.T. Opoz, X. Chen, Chip formation mechanism using finite element simulation, J. Mech. Eng. **62** (2016)
[38] K. Vivekananda, G.N. Arka, S.K. Sahoo, Finite element analysis and process parameters optimization of ultrasonic vibration assisted turning (UVT), Procedia Mater. Sci. **6**, 1906–1914 (2014)
[39] M. Asad, H. Ijaz, W. Saleem, A.S.B. Mahfouz, Z. Ahmad, T. Mabrouki, Finite element analysis and statistical optimization of end-burr in turning AA2024, Metals **9**, 1–19 (2019)
[40] W. Saleem, M. Asad, M. Zain-ul-abdein, H. Ijaz, T. Mabrouki, Numerical investigations of optimum turning parameters—AA2024-T351 aluminum alloy, Mach. Sci. Technol. **20**, 634–654 (2016)

Cite this article as: H. Ijaz, M. Danish, M. Asad, S. Rubaiee, A three-dimensional finite element-approach to investigate the optimum cutting parameters in machining AA2024, Mechanics & Industry **21**, 615 (2020)